












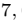


















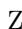


Final Results of the MAJORANA DEMONSTRATOR's Search for Double-Beta Decay of ^{76}Ge to Excited States of ^{76}Se

I.J. Arnquist,¹ F.T. Avignone III,^{2,3} A.S. Barabash ⁴ E. Blalock,^{5,6} B. Bos,^{7,6} M. Busch,^{8,6} Y.-D. Chan,⁹ J.R. Chapman ^{7,6} C.D. Christofferson ¹⁰ P.-H. Chu ¹¹ C. Cuesta ¹² J.A. Detwiler ¹³ Yu. Efremenko,^{14,3} H. Ejiri,¹⁵ S.R. Elliott ¹¹ N. Fuad ¹⁶ G.K. Giovanetti,¹⁷ M.P. Green ^{5,6,3} J. Gruszko ^{7,6} I.S. Guinn ³ V.E. Guiseppe ³ C.R. Haufe,^{7,6} R. Henning ^{7,6} D. Hervas Aguilar ^{7,6,*} E.W. Hoppe ¹ I. Kim ¹¹ † R.T. Kouzes ¹ T.E. Lannen V,² A. Li ¹⁸ R. Massarczyk ¹¹ S.J. Meijer ¹¹ T.K. Oli ¹⁹ ‡ L.S. Paudel ¹⁹ W. Pettus ¹⁶ A.W.P. Poon ⁹ D.C. Radford,³ A.L. Reine ¹⁶ K. Rielage ¹¹ D.C. Schaper ¹¹ § S.J. Schleich ¹⁶ D. Tedeschi,² R.L. Varner ³ S. Vasilyev,²⁰ S.L. Watkins ¹¹ ¶ J.F. Wilkerson ^{7,6,3} C. Wiseman ¹³ C.-H. Yu ³ and B.X. Zhu^{11,**}

(MAJORANA Collaboration)

¹*Pacific Northwest National Laboratory, Richland, WA 99354, USA*

²*Department of Physics and Astronomy, University of South Carolina, Columbia, SC 29208, USA*

³*Oak Ridge National Laboratory, Oak Ridge, TN 37830, USA*

⁴*National Research Center "Kurchatov Institute", Kurchatov Complex of Theoretical and Experimental Physics, Moscow, 117218 Russia*

⁵*Department of Physics, North Carolina State University, Raleigh, NC 27695, USA*

⁶*Triangle Universities Nuclear Laboratory, Durham, NC 27708, USA*

⁷*Department of Physics and Astronomy, University of North Carolina, Chapel Hill, NC 27514, USA*

⁸*Department of Physics, Duke University, Durham, NC 27708, USA*

⁹*Nuclear Science Division, Lawrence Berkeley National Laboratory, Berkeley, CA 94720, USA*

¹⁰*South Dakota Mines, Rapid City, SD 57701, USA*

¹¹*Los Alamos National Laboratory, Los Alamos, NM 87545, USA*

¹²*Centro de Investigaciones Energéticas, Medioambientales y Tecnológicas, CIEMAT 28040, Madrid, Spain*

¹³*Center for Experimental Nuclear Physics and Astrophysics, and Department of Physics, University of Washington, Seattle, WA 98195, USA*

¹⁴*Department of Physics and Astronomy, University of Tennessee, Knoxville, TN 37916, USA*

¹⁵*Research Center for Nuclear Physics, Osaka University, Ibaraki, Osaka 567-0047, Japan*

¹⁶*Center for Exploration of Energy and Matter, and Department of Physics, Indiana University, Bloomington, IN 47405, USA*

¹⁷*Physics Department, Williams College, Williamstown, MA 01267, USA*

¹⁸*Hacıoğlu Data Science Institute, Department of Physics, University of California San Diego, CA 92093, USA*

¹⁹*Department of Physics, University of South Dakota, Vermillion, SD 57069, USA*

²⁰*Joint Institute for Nuclear Research, Dubna, 141980 Russia*

(Dated: October 15, 2024)

^{76}Ge can $\beta\beta$ decay into three possible excited states of ^{76}Se , with the emission of two or, if the neutrino is Majorana, zero neutrinos. None of these six transitions have yet been observed. The MAJORANA DEMONSTRATOR was designed to study $\beta\beta$ decay of ^{76}Ge using a low background array of high purity germanium detectors. With 98.2 kg-y of isotopic exposure, the DEMONSTRATOR sets the strongest half-life limits to date for all six transition modes. For $2\nu\beta\beta$ to the 0_1^+ state of ^{76}Se , this search has begun to probe for the first time half-life values predicted using modern many-body nuclear theory techniques, setting a limit of $T_{1/2} > 1.5 \times 10^{24}$ y (90% CL).

Double-beta ($\beta\beta$) decay is a rare second-order weak nuclear process in which two neutrons simultaneously decay to two protons and emit two electrons. $\beta\beta$ decay was predicted by Goeppert-Mayer to occur in even-even nuclei in which a single β decay is forbidden [1]. Furthermore, if the neutrino is a Majorana fermion, meaning it is its own antiparticle [2], then it is possible for neutrinoless double-beta decay ($0\nu\beta\beta$) to occur [3]. $\beta\beta$ decay with the emission of two neutrinos ($2\nu\beta\beta$) has been directly measured in 11 isotopes, with half-lives in a range of $10^{18} - 10^{22}$ yr [4]. $0\nu\beta\beta$ has not been observed, but its discovery would prove that the neutrino is a Majorana fermion [5], provide an example of lepton number violation in nature, and might provide a mechanism for the

generation of the observed matter-antimatter asymmetry in the universe [6, 7]. As a result, a robust experimental program has risen to search for $0\nu\beta\beta$ in a variety of isotopes [8–11].

$\beta\beta$ decay can cause a transition of parent nuclei to daughters in either the ground state (G.S.) or an energetically allowed excited state (E.S.) [12]. Decays to E.S.s have a lower Q-value than decays to the G.S., and they include the prompt emission of one or more γ rays. The branching ratios are suppressed for E.S. decays relative to G.S. decays, due to the smaller phase space of the decay. To date, only $\beta\beta$ transitions to the first 0^+ E.S. of two isotopes have been observed, in ^{100}Mo ($T_{1/2} = 6.7_{-0.4}^{+0.5} \times 10^{20}$ y) [13–20] and ^{150}Nd

$(T_{1/2} = 1.18_{-0.20}^{+0.23} \times 10^{20} \text{ y})$ [21–25].

Applying Fermi's golden rule and the closure approximation, we can express the half-life for $2\nu\beta\beta$ as:

$$T_{1/2}^{-1} = G_{d.s.}^{2\nu} \cdot (g_A^{eff,2\nu})^4 \cdot |M_{d.s.}^{2\nu}|^2 \quad (1)$$

where $G_{d.s.}^{2\nu}$ is the phase space factor (PSF), which depends on the daughter nuclear state, $(g_A^{eff,2\nu})^2$ is the axial vector coupling constant with an empirical quenching term applied, and $|M_{d.s.}^{2\nu}|$ is the nuclear matrix element. The PSF can be accurately calculated [26–28], but there is large uncertainty on $(g_A^{eff,2\nu})^4 \cdot |M_{d.s.}^{2\nu}|^2$ [29]; this means that half-life measurements of $2\nu\beta\beta$ to both the G.S. and E.S.s serve as useful tests of nuclear many-body models used to compute the nuclear matrix element. In addition, the nuclear matrix element for $2\nu\beta\beta$ transitions to 2^+ states is sensitive to a bosonic component of the neutrino wave function [30, 31].

For $0\nu\beta\beta$ when dominated by light neutrino exchange, the half-life can be expressed as:

$$T_{1/2}^{-1} = G^{0\nu} \cdot (g_A^{eff,0\nu})^4 |M^{0\nu}|^2 \langle m_{\beta\beta} \rangle^2 \quad (2)$$

where $m_{\beta\beta}$ is the effective Majorana mass of the electron neutrino, a coherent average of the neutrino masses. Given an accurate calculation of $(g_A^{eff,0\nu})^4 |M^{0\nu}|^2$, a measurement of the $0\nu\beta\beta$ half-life would provide information about the neutrino mass and Majorana CP-phases [32]. Furthermore, the branching ratio for $\beta\beta$ decay modes to E.S.s can vary depending on the physics mechanisms; this means that a measurement of $0\nu\beta\beta$ to an E.S. of the daughter nucleus could help inform how to extend the Standard Model in order to accommodate Majorana neutrinos [33].

^{76}Ge is a promising isotope with an active experimental program for measuring $\beta\beta$ decay [34]. Arrays of high purity germanium (HPGe) detectors manufactured from germanium that has been isotopically enriched in ^{76}Ge are capable of achieving high detection efficiency, an ultra-low background rate, and excellent energy resolution. The MAJORANA DEMONSTRATOR [35], which operated HPGe detectors in vacuum, and GERDA [36], which operated HPGe detectors submerged in liquid argon instrumented to act as an active veto, both recently completed their data-taking campaigns and achieved the two lowest background indices and best energy resolutions in their searches for $0\nu\beta\beta$ out of any experiments performed to date.

^{76}Ge can decay into three E.S.s of ^{76}Se with a decay structure shown in Fig. 1; these transitions have never been observed before. Searches for E.S. decay modes were performed by both the DEMONSTRATOR [37] and GERDA [38] by searching for peaks produced when the deexcitation γ rays escape the detector of origin and are fully absorbed in a second HPGe detector.

The MAJORANA DEMONSTRATOR searched for $0\nu\beta\beta$

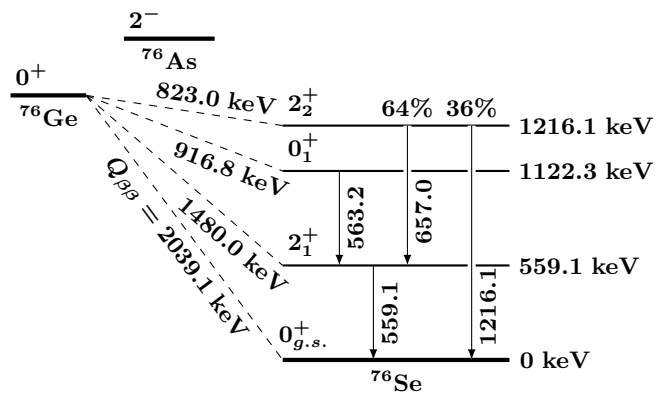


FIG. 1. Level diagram for $\beta\beta$ decay of ^{76}Ge to ^{76}Se .

and $\beta\beta$ decay to E.S. using an array of HPGe detectors. The experiment consisted of two modules, each of which consisted of an array of HPGe detectors operated in a separate vacuum cryostat. The modules were constructed from ultra-low background materials [39, 40] and placed in a low-background passive shield, surrounded by a muon veto with nearly 4π -coverage [41, 42]. For each module, a ^{228}Th line source was stored outside of this shield and deployed once per week along a helical track surrounding the cryostat to calibrate the detectors [43]. The experiment was located at the 4850 ft level (4300 m.w.e.) in the Davis campus of the Sanford Underground Research Facility, in Lead, SD [44].

The DEMONSTRATOR utilized three types of p-type HPGe detector geometries, each of which had a p^+ -type point-like electrode on one face, and an n^+ -type electrode on the other surfaces. These detector geometries were chosen for their excellent energy resolution and for their ability to discriminate single- and multi-site events using pulse-shape discrimination (PSD) techniques. Most of the detectors (up to 35 detectors totalling 29.7 kg) were p-type point-contact (PPC) detectors [45], with an isotopic fraction of 87.4% ^{76}Ge . In addition, up to 23 BEGeTM detectors [46] totalling 14.4 kg were used, with a natural isotopic abundance of 7.8% ^{76}Ge . Near the end of the DEMONSTRATOR's operation for $0\nu\beta\beta$, 4 inverted coaxial point contact (ICPC) detectors [47] were installed, totalling 6.7 kg, with an isotopic fraction of 88% ^{76}Ge .

Module 1 began operation in its low background configuration in December 2015, and Module 2 began in August 2016. For this analysis, we divide data into five datasets, listed in Tab. II, based on major hardware changes; these are combinations of the 13 datasets described in Ref. [35]. We exclude a period from Oct. 2016 to Jan. 2017 with higher electronic noise due to sub-optimal grounding. During most of its operation, blinding was applied via data parsing, with cycles of 31 h of open data followed by 93 h of blind data.

Signals from the HPGe detectors were digitized [48] and analyzed on-disk. Each detector was read out using two channels with differing gains; the high-gain channels had a dynamic range up to ~ 3 MeV and the low-gain channels had a dynamic range up to ~ 10 MeV. Each digitizer channel was triggered independently using an internal trapezoidal filter, typically with energy thresholds of < 1 keV for the high-gain channels. Waveform energies are corrected for digitizer non-linearity [49] and charge-trapping [50], and were calibrated once per week using Th-chain gamma peaks [51].

The detection signature used to identify $\beta\beta$ to E.S.s is to search for energy peaks created by the full absorption of a gamma in a detector different from the site of the decay. This signature directly takes advantage of the DEMONSTRATOR's strength in peak searches, which derives from its excellent energy resolution and operation in vacuum cryostats. Because the site of the decay will be inside of a detector, we can expect a typical event following this signature to involve multiple detector hits in coincidence; thus, we reject events with a detector multiplicity of 1. $\beta\beta$ to E.S. events with multiplicity 1 will produce a broad spectral signal. Since the spectral signal from $2\nu\beta\beta$ to the G.S. will be a large background for this feature we would gain little sensitivity from this signal compared to our selected signature; in addition, analysis of broad spectral features is subject to greater systematic uncertainties from the modelling of backgrounds to which this peak search analysis is immune.

Detector hits that fall within a rolling $4 \mu\text{s}$ window are combined into events, with event multiplicity defined as the number of HPGe detector hits in a single event. Most hits have data from both the high and low gain channels; the signal from the high-gain channels were preferentially used for the analysis, unless the energy surpassed the dynamic range or the high gain channel did not have a trigger that passed all data cleaning cuts while the low gain did; if both channels fail data cleaning cuts the entire event is rejected. In addition, we reject events that occur during periods of high microphonic noise during fills of the LN dewars used to cool the cryostats, and within 20 ms before and 1 s after a muon event, removing $< 1\%$ of events [42, 52]. Additional digital signal processing algorithms are used to remove non-physical events, keeping $> 99.9\%$ of physics events. High multiplicity events also contain valuable information from multiple detectors which we can use to achieve a large reduction in backgrounds. Similar techniques were used for each E.S. transition, and any differences will be noted. This analysis technique was also used in Ref. [37]; since then, multiple refinements have been made to further improve sensitivity, which will be noted. The background rejection cuts were developed and optimized using open data.

We use simulations to estimate the detection efficiency of these peaks including the effect of background cuts, and to optimize the tradeoff between signal sacrifice and

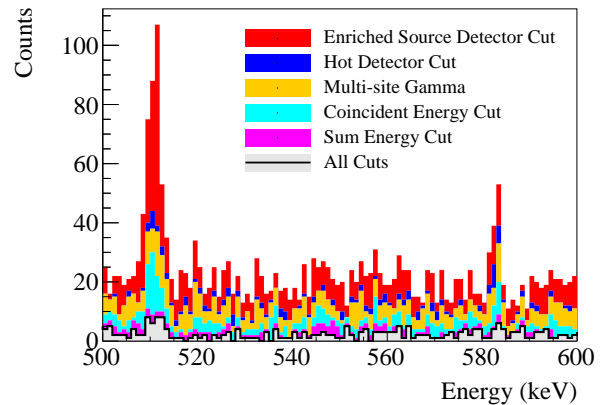


FIG. 2. Energy spectrum for high multiplicity events from full dataset. The background reduction cuts are applied in the order listed in the legend.

background reduction in order to boost our sensitivity. MaGe [53] is a Geant4 [54] based software library that implements the full as-built geometry for each experimental configuration of the MAJORANA DEMONSTRATOR and produces Monte-Carlo simulations of a variety of physical processes. To generate $\beta\beta$ decays to E.S.s, the DECAY0 [55] library was used, with several modifications. DECAY0 was modified to include angular correlations in the deexcitation γ rays from the 2^+_{21} E.S. of ^{76}Se (the angular correlation for the 0^+_{11} E.S. was already included), and the precision of the energy values used to generate γ rays was increased, from 559 to 559.101 keV, from 563 to 563.178 keV, and from 1216 to 1216.104 keV [56]. For other radioactive backgrounds and calibration source simulations, the standard radioactive decay module built into Geant4 was used to generate events.

Step data produced by Geant4 is post-processed to simulate the observables produced by HPGe detectors. This stage simulates the effect of dead time from detectors that are disabled or unstable, from data cleaning cuts, and from hardware retriggering by randomly rejecting detector hits in proportion with the time spent in that configuration. The effect of transition dead layers is simulated by reducing the energy for steps in the transition layers caused by low charge collection efficiency within ~ 1 mm of the n^+ detector surfaces. One hundred separate sets of post-processed simulations are produced for each dataset and E.S. decay mode, varying the transition dead layer parameters to study the systematic effect from uncertainty in the dead layer thickness. In addition, a background model simulation is produced by sampling from about 100 post-processed simulations of a variety of isotopes in different hardware components, in proportion with the fitted activities from Ref. [57].

We apply a sequence of background reduction cuts, determined based on our simulations to improve the sensitivity of the experiment. The “Enriched Source De-

ector Cut” rejects hits that are not in coincidence with an enriched detector. The “Hot Detector Cut” rejects events that include one of two detectors closest to the Module 1 crossarm; this cut was not included in Ref. [37]. These detectors have significantly elevated background rates consistent with ^{232}Th progeny in a cavity in the interface between the Module 1 cryostat cold plate and crossarm [57, 58]. For $\beta\beta$ to the 2_1^+ E.S. and 2_2^+ E.S. with the emission of a 1216 keV γ ray, we additionally require that an event has a multiplicity of exactly 2, since these modes only emit a single γ ray.

Because γ rays that are fully absorbed inside a detector typically Compton scatter at least once, we use the $AvsE$ PSD parameter to select for multi-site events [59]. $AvsE$ uses a comparison between the current amplitude (A) and energy (E) of a pulse to discriminate between single- and multi-site events; multi-site events usually have a lower A for a given E in point-contact HPGe detectors relative to single-site events. $AvsE$ is calibrated to measure 90% single-site events in the ^{208}Tl double-escape peak (DEP), and is corrected for correlations with drift time and energy [35]. Because of the difficulty of simulating the effect of $AvsE$ for a wide variety of energies and event topologies, we instead calculate this cut efficiency for each peak using ^{228}Th calibration data. We measure the multi-site acceptance of 16 full energy peaks (FEPs) in the range of 400 keV to 1700 keV, and model dependence on energy (E_{FEP}) as

$$\varepsilon_{AvsE}(E_{FEP}; p_0, p_1) = p_0 - \frac{p_1}{E_{FEP}} \quad (3)$$

We perform best fit of the parameters $p_0 \simeq 0.92$ and $p_1 \simeq 3.4 \times 10^4$ keV over all detectors and calibration runs for each dataset, and the fit performs well with a χ^2 value ranging from 10-20 for 14 d.o.f. We additionally check for a systematic effect based on the incidence angle of γ rays using the acceptance of the 511 keV annihilation peak in coincidence with a DEP or single-escape peak (SEP) event, which originates inside of detectors instead of from the calibration track; this is consistent with the above model. We also check for variance over time in the DEP, SEP, and Compton continuum and in variance between the acceptance in many detectors of the 583 keV FEP; these are used to calculate systematic uncertainty terms, with the dominant uncertainty arising from variance over time. Based on this, we measure an acceptance of $80.9 \pm 0.2\%$ for the 559 and 563 keV γ rays from the 0_1^+ E.S. of ^{76}Se . This cut was not used in Ref. [37].

The last set of cuts we apply are the Coincident- and Sum-Energy cuts, which reject events where either the sum over all hits or any hit in a coincident detector fall within a set of energy ranges. These cuts are designed to reject multi-detector events from γ ray cascades and Compton-scattered γ rays from common backgrounds, respectively. The energy ranges were determined algorithmically to optimize the discovery sensitivity of the

Cut Description	ε_{signal}	$\varepsilon_{background}$
Gamma FEP Efficiency	5.4%	—
Multiplicity ≥ 2	71.5%	8.0%
Enriched Source Detector Cut	97.5%	63.6%
Hot Detector Cut	97.4%	88.9%
Multi-site Gamma	80.9%	56.2%
Coincident Energy Cut	82.6%	54.8%
Sum Energy Cut	88.8%	56.9%
Total	2.2%	0.8%

TABLE I. Summary of the effect of each analysis cut when applied to the search for $2\nu\beta\beta$ to the 0_1^+ E.S. of ^{76}Se , in the order listed. The signal acceptance ε_{signal} is the exposure-weighted average across datasets, calculated from simulations. The background acceptance $\varepsilon_{background}$ is calculated from the events rejected in the fit window for all datasets (see Fig. 2).

experiment, based on the signal and background acceptance efficiencies determined using simulations of the E.S. modes and of the background model. The events were binned both by sum- and coincident hit energies, and bins were added to the cut if doing so improved the sensitivity. To avoid statistical biases towards cutting statistical fluctuations in the simulations, a new energy range was only introduced to the cut if we estimated it to have a $> 97\%$ chance of improving sensitivity. For the $0\nu\beta\beta$ decay to the 2_1^+ and the single- γ branch of the 2_2^+ mode, we do not apply this algorithm; instead we only apply a coincident energy cut around the $Q_{\beta\beta}$ -value of the decays since the coincident energy spectrum is strongly peaked.

The effect of the cuts for $\beta\beta$ to the 0_1^+ E.S. is shown in Tab. I and Fig. 2, and the final detection efficiency for each decay mode can be seen in Tab. III. These were determined by measuring the efficiency in simulations and multiplying the $AvsE$ efficiency determined for each energy peak. One source of systematic uncertainty is derived from the variance introduced by changing the simulation post-processing parameters, measured to be 0.06%; the dominant source of uncertainty arises from the thickness of the dead layer. In addition, uncertainty in the spectral shape from DECAY0 was estimated by performing a Kolmogorov-Smirnov test comparing the G.S. spectrum to a more precise determination from Ref. [26]; this was found to be 0.01%. Finally, because of the reliance on simulations to calculate the detection efficiency, we validate the simulations using DEPs in coincidence with full absorption of a 511 keV annihilation γ as proxies for $\beta\beta$ to E.S.s, since these events originate from inside of detectors. To do this, we use data collected using a ^{56}Co line source that was inserted into each calibration track for a period of one week; this source emits many high-energy γ rays, and we used 6 DEPs and 7 SEPs. To validate the simulation, we compared the measured ratio of the peak amplitudes for events in coincidence with a 511 keV hit and for multiplicity 1 hits. We found an average disagreement in this ratio of 2.2%, with a significant difference of 8.4% in DEPs in Module 1. The source

Dataset	Time	Efficiency Period	Exposure (kg-y)	BG Index (cts/keV-kg-y)
DS I M1	7/15-10/15	2.04(24)%	1.92(1)	0.056(23)
DS II M1	12/15-8/16	2.12(24)%	5.02(3)	0.021(9)
DS III M1	8/16-11/19	2.83(25)%	39.68(22)	0.028(4)
DS III M2	8/16-11/19	0.99(22)%	30.90(16)	0.012(3)
DS IV M1	11/19-8/20	2.07(25)%	7.36(4)	0.015(6)
DS V M1	8/20-3/21	2.30(24)%	7.14(4)	0.023(8)
DS V M2	8/20-3/21	3.62(27)%	6.14(4)	0.018(7)

TABLE II. Detection efficiency for $\beta\beta$ decay of ^{76}Ge to 0_1^+ E.S. of ^{76}Se , isotopic exposure, and best-fit background index for each dataset (DS)/module (M)

of this disagreement cannot be explained by effects such as dead layers, so we include it as a systematic uncertainty term, which scales to 0.23%; this is our dominant uncertainty.

The measured half-life is calculated using

$$T_{1/2} = \frac{\ln 2 N_A \varepsilon M_{iso} T_{live}}{m_{76} \langle s \rangle} \quad (4)$$

where N_A is avogadro's number, $m_{76} = 75.9$ g is the molar mass of ^{76}Ge , and $\langle s \rangle$ is the estimated combined amplitude of the signal peaks. The isotopic exposure $M_{iso} T_{live} = 98.2 \pm 0.5$ kg-y is the product of the total mass of ^{76}Ge in a module times the operating time of the module summed over datasets. Note that this differs from the active exposure defined in Ref. [35] which includes all Ge in active regions of the detector and subtracts dead time; instead, these effects are included as reductions in detection efficiency, and variation in the number of active detectors is the primary driver for the variation in efficiency between datasets seen in Tab. II.

We use a profile likelihood analysis to construct Neyman confidence intervals for the half-life of each E.S. decay mode. The data are modelled using one or more peaks, using the measured peakshape function, on a flat background; we also include nuisance parameters for uncertainty in the detection efficiency, drift in the peak position, and uncertainty in the peak width. The model is applied for events in an energy range of 520 – 575 keV for the 559- and 563-keV peaks, 620 – 690 keV for the 657 keV peak, omitting 660 – 670 keV to remove a U-chain peak, and 1180 – 1300 keV for the 1216 keV peak, omitting 1230 – 1245 keV to remove another U-chain peak. For each dataset, we independently calculate the exposure and detection efficiency, and we float an independent background index. This is done due to the large variations based on which detectors were enabled; most noticeably, the efficiency and backgrounds both increased significantly in Module 2 after the upgrade resulted in almost all detectors being active. We use an extended unbinned likelihood function, implemented with iminuit [60], to calculate our confidence intervals. For the 2_2^+ decay modes, we simultaneously profile over all three peaks. Wilks' theorem is applied to calculate p-values

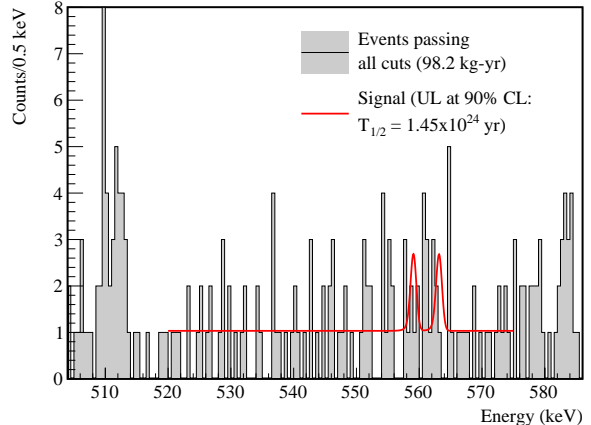


FIG. 3. Energy spectrum for events passing all cuts for $2\nu\beta\beta$ to the 0_1^+ E.S.. In red, the modelled signal assuming a half-life at the 90% CL limit and the best-fit mean background.

for all modes except for the $0\nu\beta\beta$ to 2_1^+ , which had zero counts in the background window; in this case, p-values were calculated through Monte-Carlo sampling. For all $\beta\beta$ to E.S. decay modes, we measure a null result, with detailed results shown in Tab. III.

Combined with the measured half-life for $2\nu\beta\beta$ to the G.S. of ^{76}Se of $T_{1/2} = 2.05_{-0.05}^{+0.04} \text{ syst} \pm 0.01 \text{ stat} \times 10^{21}$ yr [57], the limit for the 0_1^+ E.S. corresponds to a branching ratio of $\text{BR} < 0.0014$ (sensitivity of $\text{BR} < 0.0009$). We compare this BR limit to predictions using theoretical calculations of the PSFs [28] and nuclear matrix elements, under the assumption that the same value for $g_A^{eff,2\nu}$ applies to each daughter state, using $\text{BR} = \frac{G_{E.S.}^{2\nu} |M_{E.S.}^{2\nu}|^2}{G_{G.S.}^{2\nu} |M_{G.S.}^{2\nu}|^2}$. Several variants of Quasiparticle Random Phase Approximation (QRPA) have been applied [61–63], with the minimum predicted BR of 0.0045 strongly disfavored with a P-value of 1×10^{-5} . An Effective Theory (ET) predicted a BR of 0.0011-0.0012 [64], which is disfavored with a p-value of 0.23. The Nuclear Shell Model (NSM) predicted a BR of 0.00068-0.00076 [38] and the Interacting Boson Model (IBM2) predicted 0.00025-0.00027 [65], both beyond the sensitivity of this search. For $2\nu\beta\beta$ to the 2_1^+ E.S., BR predictions range from $4.2 \times 10^{-7} - 2.1 \times 10^{-6}$ [64, 66, 67], well beyond the sensitivity of this search.

The MAJORANA DEMONSTRATOR has set the most stringent limits to date for all E.S. decay modes in ^{76}Ge . We achieved sensitivity to half-life values for $2\nu\beta\beta$ to the 0_1^+ state of ^{76}Se in a range predicted by recent calculations. We have benefited from the excellent energy resolution of the experiment and from operating the detectors in vacuum. Future experimental efforts from the LEGEND collaboration [34] will use detectors operated in a liquid argon active veto, which will increase shield-

Decay Mode	Peak Energies (keV)	Peak FWHM (keV)	Efficiency	$\langle s \rangle$ BF	$\langle s \rangle$ Limit	$T_{1/2}$ Limit	$T_{1/2}$ Sensitivity
$0_{g.s.}^+ \xrightarrow{2\nu\beta\beta} 0_1^+$	559.1, 563.2	1.12, 1.13	2.15(24)%	1.3	8.0	1.5×10^{24} y	2.2×10^{24} y
$0_{g.s.}^+ \xrightarrow{2\nu\beta\beta} 2_1^+$	559.1	1.12	1.15(26)%	0.0	2.1	3.0×10^{24} y	2.1×10^{24} y
$0_{g.s.}^+ \xrightarrow{2\nu\beta\beta} 2_2^+$	559.1, 657.0, 1216.1	1.12, 1.22, 1.73	1.76(29)%	2.1	10.9	0.88×10^{24} y	1.5×10^{24} y
$0_{g.s.}^+ \xrightarrow{0\nu\beta\beta} 0_1^+$	559.1, 563.2	1.12, 1.13	2.83(32)%	0.0	2.0	7.6×10^{24} y	5.9×10^{24} y
$0_{g.s.}^+ \xrightarrow{0\nu\beta\beta} 2_1^+$	559.1	1.12	1.58(35)%	0.0	2.5	3.5×10^{24} y	3.5×10^{24} y
$0_{g.s.}^+ \xrightarrow{0\nu\beta\beta} 2_2^+$	559.1, 657.0, 1216.1	1.12, 1.22, 1.73	2.16(32)%	0.0	1.7	6.6×10^{24} y	4.3×10^{24} y

TABLE III. Results for each $\beta\beta$ -transition of ^{76}Ge to an E.S. of ^{76}Se . Peak FWHM and efficiency averaged over datasets, estimated counts (s) from best fit (BF) and upper limit, and half-life limit and sensitivity at 90% C.L. are shown.

ing between detectors and introduce backgrounds from ^{42}K ; thus, LEGEND will likely require new analysis techniques to significantly improve on this result.

This material is based upon work supported by the U.S. Department of Energy, Office of Science, Office of Nuclear Physics under contract / award numbers DE-AC02-05CH11231, DE-AC05-00OR22725, DE-AC05-76RL0130, DE-FG02-97ER41020, DE-FG02-97ER41033, DE-FG02-97ER41041, DE-SC0012612, DE-SC0014445, DE-SC0017594, DE-SC0018060, DE-SC0022339, and LANLEM77/LANLEM78. We acknowledge support from the Particle Astrophysics Program and Nuclear Physics Program of the National Science Foundation through grant numbers MRI-0923142, PHY-1003399, PHY-1102292, PHY-1206314, PHY-1614611, PHY-13407204, PHY-1812409, PHY-1812356, PHY-2111140, and PHY-2209530. We gratefully acknowledge the support of the Laboratory Directed Research & Development (LDRD) program at Lawrence Berkeley National Laboratory for this work. We gratefully acknowledge the support of the U.S. Department of Energy through the Los Alamos National Laboratory LDRD Program, the Oak Ridge National Laboratory LDRD Program, and the Pacific Northwest National Laboratory LDRD Program for this work. We gratefully acknowledge the support of the South Dakota Board of Regents Competitive Research Grant. We acknowledge the support of the Natural Sciences and Engineering Research Council of Canada, funding reference number SAPIN-2017-00023, and from the Canada Foundation for Innovation John R. Evans Leaders Fund. We acknowledge support from the 2020/2021 L'Oréal-UNESCO for Women in Science Programme. This research used resources provided by the Oak Ridge Leadership Computing Facility at Oak Ridge National Laboratory and by the National Energy Research Scientific Computing Center, a U.S. Department of Energy Office of Science User Facility. We thank our hosts and colleagues at the Sanford Underground Research Facility for their support.

* Present address: Technical University of Munich, 85748 Garching, Germany

† Present address: Lawrence Livermore National Laboratory, Livermore, CA 94550, USA

‡ Present address: Argonne National Laboratory, Lemont, IL 60439, USA

§ Present address: Indiana University, Bloomington, IN 47405, USA

¶ Present address: Pacific Northwest National Laboratory

** Present address: Jet Propulsion Laboratory, California Institute of Technology, Pasadena, CA 91109, USA

- [1] M. Goeppert-Mayer, Double beta-disintegration, *Phys. Rev.* **48**, 512 (1935).
- [2] E. Majorana, Teoria simmetrica dell'elettrone e del positrone, *Il Nuovo Cimento* (1924-1942) **14**, 171 (2008).
- [3] W. H. Furry, On transition probabilities in double beta-disintegration, *Phys. Rev.* **56**, 1184 (1939).
- [4] A. Barabash, Precise half-life values for two-neutrino double- β decay: 2020 review, *Universe* **6**, 159 (2020).
- [5] J. Schechter and J. W. F. Valle, Neutrinoless double- β decay in $SU(2) \times U(1)$ theories, *Phys. Rev. D* **25**, 2951 (1982).
- [6] A. D. Sakharov, Violation of CP Invariance, C Asymmetry, and Baryon Asymmetry of the Universe, *Pisma Zh. Eksp. Teor. Fiz.* **5**, 32 (1967).
- [7] M. Fukugita and T. Yanagida, Baryogenesis without grand unification, *Phys. Lett. B* **174**, 45 (1986).
- [8] M. J. Dolinski, A. W. Poon, and W. Rodejohann, Neutrinoless double-beta decay: Status and prospects, *Annual Review of Nuclear and Particle Science* **69**, 219 (2019).
- [9] J. J. Gómez-Cadenas, J. Martín-Albo, J. Menéndez, M. Mezzetto, F. Monrabal, and M. Sorel, The search for neutrinoless double-beta decay, *Riv. Nuovo Cimento* **46**, 619 (2023).
- [10] A. Barabash, Double beta decay experiments: Recent achievements and future prospects, *Universe* **9**, 290 (2023).
- [11] M. Agostini, G. Benato, J. A. Detwiler, J. Menéndez, and F. Vissani, Toward the discovery of matter creation with neutrinoless $\beta\beta$ decay, *Rev. Mod. Phys.* **95**, 025002 (2023).
- [12] P. Belli, R. Bernabei, F. Cappella, V. Caracciolo, R. Cerulli, A. Incicchitti, and V. Merlo, Double beta decay to excited states of daughter nuclei, *Universe* **6**, 239 (2020).
- [13] A. Barabash, F. Avignone, J. Collar, C. Guerard, R. Arthur, R. Brodzinski, H. Miley, J. Reeves, J. Meier,

- K. Ruddick, and V. Umatov, Two neutrino double-beta decay of ^{100}Mo to the first excited 0^+ state in ^{100}Ru , *Physics Letters B* **345**, 408 (1995).
- [14] A. Barabash, R. Gurriaran, F. Hubert, P. Hubert, and V. Umatov, $2\nu\beta\beta$ decay of ^{100}Mo to the first 0^+ excited state in ^{100}Ru , *Phys. At. Nucl.* **62**, 2039 (1999).
- [15] L. De Braekeleer, M. Hornish, A. Barabash, and V. Umatov, Measurement of the $\beta\beta$ -decay rate of ^{100}Mo to the first excited 0^+ state of ^{100}Ru , *Phys. Rev. Lett.* **86**, 3510 (2001).
- [16] R. Arnold *et al.*, Measurement of double beta decay of ^{100}Mo to excited states in the NEMO 3 experiment, *Nuclear Physics A* **781**, 209 (2007).
- [17] M. Kidd, J. Esterline, W. Tornow, A. Barabash, and V. Umatov, New results for double-beta decay of ^{100}Mo to excited final states of ^{100}Ru using the TUNL-ITEP apparatus, *Nuclear Physics A* **821**, 251 (2009).
- [18] New observation of $2\beta2\nu$ decay of ^{100}Mo to the 0_1^+ level of ^{100}Ru in the ARMONIA experiment, *Nuclear Physics A* **846**, 143 (2010).
- [19] R. Arnold *et al.*, Investigation of double beta decay of ^{100}Mo to excited states of ^{100}Ru , *Nuclear Physics A* **925**, 25 (2014).
- [20] C. Augier *et al.* (CUPID-Mo Collaboration), New measurement of double- β decays of ^{100}Mo to excited states of ^{100}Ru with the cupid-mo experiment, *Phys. Rev. C* **107**, 025503 (2023).
- [21] A. S. Barabash, F. Hubert, P. Hubert, and V. I. Umatov, Double beta decay of ^{150}Nd to the first 0^+ excited state of ^{150}Sm , *JETP Lett.* **79**, 10 (2004).
- [22] A. S. Barabash, P. Hubert, A. Nachab, and V. I. Umatov, Investigation of $\beta\beta$ decay in ^{150}Nd and ^{148}Nd to the excited states of daughter nuclei, *Phys. Rev. C* **79**, 045501 (2009).
- [23] M. F. Kidd, J. H. Esterline, S. W. Finch, and W. Tornow, Two-neutrino double- β decay of ^{150}Nd to excited final states in ^{150}Sm , *Phys. Rev. C* **90**, 055501 (2014).
- [24] O. G. Polischuk, A. S. Barabash, P. Belli, R. Bernabei, R. S. Boiko, F. Cappella, V. Caracciolo, R. Cerulli, F. A. Danevich, A. D. Marco, A. Incicchitti, D. V. Kasperovych, V. V. Kobychov, S. I. Kononov, M. Laubenstein, D. V. Poda, V. I. Tretyak, and V. I. Umatov, Double beta decay of ^{150}Nd to the first 0^+ excited level of ^{150}Sm , *Physica Scripta* **96**, 085302 (2021).
- [25] X. Aguerre *et al.*, Measurement of the double- β decay of ^{150}Nd to the 0_1^+ excited state of ^{150}Sm in NEMO-3, *Eur. Phys. J. C* **83**, 10.1140/epjc/s10052-023-12227-x.
- [26] J. Kotila and F. Iachello, Phase-space factors for double- β decay, *Phys. Rev. C* **85**, 034316 (2012).
- [27] A. Neacsu and M. Horoi, An effective method to accurately calculate the phase space factors for $\beta^-\beta^-$ decay, *Advances in High Energy Physics* **2016**, 7486712 (2016).
- [28] S. Stoica and M. Mirea, Phase space factors for double-beta decays, *Frontiers in Physics* **7**, 12 (2019).
- [29] J. T. Suhonen, Value of the axial-vector coupling strength in β and $\beta\beta$ decays: A review, *Front. Phys.* **5**, 10.3389/fphy.2017.00055 (2017), cited by: 148; All Open Access, Gold Open Access, Green Open Access.
- [30] A. Dolgov and A. Smirnov, Possible violation of the spin-statistics relation for neutrinos: Cosmological and astrophysical consequences, *Phys. Lett. B* **621**, 1 (2005).
- [31] A. Barabash, A. Dolgov, R. Dvornický, F. Šimkovic, and A. Smirnov, Statistics of neutrinos and the double beta decay, *Nucl. Phys. B* **783**, 90 (2007).
- [32] J. Engel and J. Menéndez, Status and future of nuclear matrix elements for neutrinoless double-beta decay: a review, *Reports on Progress in Physics* **80**, 046301 (2017).
- [33] F. Šimkovic and A. Faessler, Distinguishing the $0\nu\beta\beta$ -decay mechanisms, *Prog. Part. Nucl. Phys.* **48**, 201 (2002).
- [34] N. Abgrall *et al.* (LEGEND Collaboration), LEGEND-1000 preconceptual design report (2021), arXiv:2107.11462 [nucl-ex].
- [35] I. J. Arnquist *et al.* (MAJORANA Collaboration), Final result of the MAJORANA DEMONSTRATOR's search for neutrinoless double- β decay in ^{76}Ge , *Phys. Rev. Lett.* **130**, 062501 (2023).
- [36] M. Agostini *et al.* (GERDA Collaboration), Final results of GERDA on the search for neutrinoless double- β decay, *Phys. Rev. Lett.* **125**, 252502 (2020).
- [37] I. J. Arnquist *et al.* (MAJORANA Collaboration), Search for double- β decay of ^{76}Ge to excited states of ^{76}Se with the MAJORANA DEMONSTRATOR, *Phys. Rev. C* **103**, 015501 (2021).
- [38] M. Agostini *et al.* (GERDA Collaboration), $2\nu\beta\beta$ decay of ^{76}Ge into excited states with GERDA phase I, *Journal of Physics G: Nuclear and Particle Physics* **42**, 115201 (2015).
- [39] E. Hoppe, C. Aalseth, O. Farmer, T. Hossbach, M. Liezers, H. Miley, N. Overman, and J. Reeves, Reduction of radioactive backgrounds in electroformed copper for ultra-sensitive radiation detectors, *Nucl. Instrum. Methods Phys. Res. A* **764**, 116 (2014).
- [40] N. Abgrall *et al.* (MAJORANA Collaboration), The MAJORANA DEMONSTRATOR radioassay program, *Nucl. Instrum. Methods Phys. Res. A* **828**, 22 (2016).
- [41] W. Bugg, Y. Efremenko, and S. Vasilyev, Large plastic scintillator panels with WLS fiber readout: Optimization of components, *Nucl. Instrum. Methods Phys. Res. A* **758**, 91 (2014).
- [42] N. Abgrall *et al.* (MAJORANA Collaboration), Muon flux measurements at the davis campus of the sanford underground research facility with the MAJORANA DEMONSTRATOR veto system, *Astroparticle Physics* **93**, 70 (2017).
- [43] N. Abgrall *et al.* (MAJORANA Collaboration), The MAJORANA DEMONSTRATOR calibration system, *Nucl. Instrum. Methods Phys. Res. A* **872**, 16 (2017).
- [44] J. Heise, The Sanford Underground Research Facility at Homestake, *Journal of Physics: Conference Series* **606**, 012015 (2015).
- [45] P. S. Barbeau, J. I. Collar, and O. Tench, Large-mass ultralow noise germanium detectors: performance and applications in neutrino and astroparticle physics, *J. Cosmol. Astropart. Phys.* **2007** (09), 009.
- [46] Canberra Industries Inc. (now Mirion Technologies), 800 Research Parkway Meriden, CT 06450, <https://www.mirion.com/products/bege-broad-energy-germanium-detectors>.
- [47] R. Cooper, D. Radford, P. Hausladen, and K. Lagergren, A novel HPGe detector for gamma-ray tracking and imaging, *Nucl. Instrum. Methods Phys. Res. A* **665**, 25 (2011).
- [48] I. J. Arnquist *et al.* (MAJORANA Collaboration), The MAJORANA DEMONSTRATOR readout electronics system, *JINST* **17** (05), T05003.
- [49] N. Abgrall *et al.* (MAJORANA Collaboration), ADC Non-linearity Correction for the MAJORANA DEMONSTRATOR,

- IEEE Trans. Nucl. Sci. **68**, 359 (2021).
- [50] I. J. Arnquist *et al.* (MAJORANA Collaboration), Charge trapping correction and energy performance of the MAJORANA DEMONSTRATOR, Phys. Rev. C **107**, 045503 (2023).
- [51] I. Arnquist *et al.* (MAJORANA collaboration), Energy calibration of germanium detectors for the MAJORANA DEMONSTRATOR, Journal of Instrumentation **18** (09), P09023.
- [52] I. J. Arnquist *et al.* (MAJORANA Collaboration), Signatures of muonic activation in the MAJORANA DEMONSTRATOR, Phys. Rev. C **105**, 014617 (2022).
- [53] M. Boswell *et al.*, MaGe-a Geant4-Based Monte Carlo Application Framework for Low-Background Germanium Experiments, IEEE Trans. Nucl. Sci. **58**, 1212 (2011).
- [54] S. Agostinelli *et al.* (Geant4 Collaboration), Geant4—a simulation toolkit, Nuclear Instruments and Methods in Physics Research Section A: Accelerators, Spectrometers, Detectors and Associated Equipment **506**, 250 (2003).
- [55] O. A. Ponkratenko, V. I. Tretyak, and Y. G. Zdesenko, Event generator DECAY4 for simulating double-beta processes and decays of radioactive nuclei, Physics of Atomic Nuclei **63**, 1282 (2000).
- [56] B. Singh, Nuclear data sheets update for $A = 76$, Nuclear Data Sheets **74**, 63 (1995).
- [57] A. Reine, *A Radiogenic Background Model for the MAJORANA DEMONSTRATOR*, Ph.D. thesis, University of North Carolina at Chapel Hill (2023).
- [58] C. Haufe, *A Study of MAJORANA DEMONSTRATOR Backgrounds with Bayesian Statistical Modeling*, Ph.D. thesis, University of North Carolina at Chapel Hill (2023).
- [59] S. I. Alvis *et al.* (MAJORANA Collaboration), Multisite event discrimination for the MAJORANA DEMONSTRATOR, Phys. Rev. C **99**, 065501 (2019).
- [60] H. Dembinski and P. O. et al., scikit-hep/iminuit, Zenodo 10.5281/zenodo.3949207 (2020).
- [61] M. Aunola and J. Suhonen, Systematic study of beta and double beta decay to excited final states, Nuclear Physics A **602**, 133 (1996).
- [62] S. Stoica and I. Mihut, Nuclear structure calculations of two-neutrino double-beta decay transitions to excited final states, Nuclear Physics A **602**, 197 (1996).
- [63] J. Toivanen and J. Suhonen, Study of several double-beta-decaying nuclei using the renormalized proton-neutron quasiparticle random-phase approximation, Phys. Rev. C **55**, 2314 (1997).
- [64] E. A. Coello Pérez, J. Menéndez, and A. Schwenk, Gamow-teller and double- β decays of heavy nuclei within an effective theory, Phys. Rev. C **98**, 045501 (2018).
- [65] J. Barea, J. Kotila, and F. Iachello, $0\nu\beta\beta$ and $2\nu\beta\beta$ nuclear matrix elements in the interacting boson model with isospin restoration, Phys. Rev. C **91**, 034304 (2015).
- [66] S. Unlu, Quasi random phase approximation predictions on two-neutrino double beta decay half-lives to the first $2+$ state, Chinese Physics Letters **31**, 042101 (2014).
- [67] J. Kostensalo, J. Suhonen, and K. Zuber, The first large-scale shell-model calculation of the two-neutrino double beta decay of ^{76}Ge to the excited states in ^{76}Se , Phys. Lett. B **831**, 137170 (2022).